Journal of Power Sources 266 (2014) 282–290

Contents lists available at ScienceDirect

Journal of Power Sources

journal homepage: www.elsevier.com/locate/jpowsour

Redox reaction between graphene oxide and In powder to prepare In_2O_3/reduced graphene oxide hybrids for supercapacitors

Xiaoyang Xu [a], Tao Wu [a], Fengling Xia [a], Yi Li [a], Congcong Zhang [a], Lei Zhang [a], Mingxi Chen [a], Xichuan Li [a], Li Zhang [a], Yu Liu [a], Jianping Gao [a, b, *]

[a] School of Science, Tianjin University, Tianjin 300072, China
[b] Collaborative Innovation Center of Chemical Science and Engineering (Tianjin), Tianjin 300072, China

HIGHLIGHTS

- Graphene oxide can be reduced by In powder in about 30 min.
- The In^{3+} ions, the by-products during reduction, were used to obtain In_2O_3/rGO.
- The In_2O_3/rGO hybrids showed high supercapacitive performance for energy storage.

ARTICLE INFO

Article history:
Received 22 February 2014
Received in revised form
21 April 2014
Accepted 7 May 2014
Available online 21 May 2014

Keywords:
Graphene oxide
Reduction
Hybrid
Supercapacitor
Electrochemical performance

ABSTRACT

A facile and quick route for the chemical reduction of graphene oxide (GO) using In powder as a reductant has been established. The reduction of GO by In powder is traced by UV–visible absorption spectroscopy, and the obtained reduced graphene oxide (rGO) is analyzed. The In^{3+} ions produced during the reaction between the GO and the In powder are chemically transformed to In_2O_3 and then form In_2O_3/rGO hybrids. The In_2O_3/rGO hybrids are used as electrode materials and their electrochemical performance are studied using cyclic voltammetry and galvanostatic charge/discharge. The In_2O_3/rGO hybrids demonstrate excellent electrochemical performance and their highest specific capacitance is 178.8 F g^{-1} which is much higher than that of either In_2O_3 or rGO. In addition, the In_2O_3/rGO hybrids are also very stable.

1. Introduction

Since its discovery by Novoselov et al., in 2004 [1], graphene has received considerable attention due to its excellent electronic [2], thermal [3], and mechanical properties [4–7]. Graphene has a unique nanostructure composed of a flat monolayer of sp^2-bonded carbon atoms that are tightly packed into a two-dimensional honeycomb lattice and so it holds great promise for applications in many fields such as nanoelectronic devices [8], sensors [9], supercapacitors [10], and solar cells [11]. However, in order for these applications to be fully developed and exploited, an easy preparation method that can produce large amounts of high quality graphene is required.

Several approaches have been developed to produce graphene including micro-mechanical cleavage [12], chemical vapor deposition [13–15], liquid-phase exfoliation [16,17], and the thermal and chemical reduction of graphene oxide (GO) [18,19]. The chemical reduction of GO is superior to others methods because it is cost-effective, produces high-yields and is well-suited for subsequent processing requirements. Although the mechanism for the reduction of GO is not completely understood, many reductants have been developed to prepare reduced GO (rGO) such as hydrazine, hydroquinone and $NaBH_4$ [20–23]. However, these reductants are harmful to human health and the environment [24], and many attempts have been made to develop environmentally friendly reductants. For example, Fernandez-Merino et al. used vitamin C to reduce GO [25], Zhu et al. used reducing sugars as the reductant [26], and Wang et al. reduced GO using polyphenol from green tea [27]. These green methods have proven to be effective for GO reduction, but they usually require long reaction time.

* Corresponding author. School of Science, Tianjin University, Tianjin 300072, China. Fax: +86 22 274 034 75.
E-mail address: jianpinggaols@126.com (J. Gao).

http://dx.doi.org/10.1016/j.jpowsour.2014.05.051
0378-7753/

In this paper, a simple, fast and environmentally friendly route for the reduction of GO using In powder as a reductant is reported. To the best of our knowledge, the use of In powder as a reductant for GO has not been reported previously. The reduction of GO by In powder was traced by UV–visible (UV–vis) absorption spectroscopy, and the obtained rGO was analyzed with all kinds of characterization methods. In addition, the In^{3+} ions were produced during the reduction of GO by the In powder. In order to take full advantage of the by-product In^{3+} ions, the In_2O_3/rGO hybrids were prepared through the chemical reaction between In^{3+} ions and ammonia water. The In_2O_3/rGO hybrids were used as electrode materials for a supercapacitor, and their electrochemical performance was evaluated using cyclic voltammetry (CV) and galvanostatic charge/discharge (GV).

2. Experimental section

2.1. Materials

Graphite was obtained from Qingdao Graphite Factory. In powder, polyvinylpyrrolidone (PVP), ammonia water, polytetrafluoroethylene emulsion (PTFE, mass fraction = 60%), carbon black, nickel foam and all other reagents were purchased from Tianjin Chemical Reagent Co. All the chemicals were analytical grade and used as received.

2.2. Preparation of GO

GO was prepared from purified natural graphite by a modified Hummer's method [28–30].

2.3. Reduction of GO by In powder

The pH of the GO suspension was adjusted to 1.0 by adding a dilute HCl solution to a GO suspension (10 mL, 1.0 g L^{-1}) at ambient temperature. Then 10 mg of In powder was added to a mixture of the above GO suspension and 1 mL of PVP solution (1×10^{-6} M). The solution was heated at 95 °C for 1.5 h to make the GO reduce.

2.4. Preparation of In_2O_3/rGO hybrids

In a typical experiment, In powder (10 mg) was added to the GO suspension (10 mL, 1.0 g L^{-1}, pH = 1.0) in a water bath at 95 °C and allowed to react for at least 3 h in order to fully convert GO to rGO. After the In powder was depleted, ammonia water was added and the solution was stirred at room temperature for 30 min. The products were then centrifuged, rinsed with distilled water, and annealed at 300 °C for 12 h to obtain In_2O_3/rGO hybrid. The product at these conditions was defined as the In_2O_3/rGO hybrid in the following content, if no additional instructions.

The In_2O_3/rGO hybrids with the different mass percent (wt%) of In_2O_3 were also fabricated.

2.5. Characterization

The UV–vis absorption spectra of the GO and rGO suspensions were recorded with a TU-1901 UV–vis spectrophotometer. The X-ray diffraction (XRD) patterns of the samples were measured using an X-ray diffractometer (BDX3300) with a reference target: Cu Ka radiation (λ = 1.54 Å), voltage: 30 kV and current: 30 mA. The samples were measured from 10 to 80° (2θ) with steps of 4° min^{-1}. Raman measurements were performed with a Raman microscope (DXR Microscope, USA). The thermogravimetric analysis (TGA) diagrams of the samples were recorded with a Rigaku-TD-TDA analyzer with a heating rate of 10 °C min^{-1}. Prior to TGA, the samples were dried in a vacuum at 30 °C for 2 days. Elemental analysis was conducted on an X-ray photoelectron spectrometer (XPS, PHI1600 ESCA System, PERKIN ELMER, US). The In_2O_3/rGO samples for transmission electron microscopy (TEM, Tecnai G2 F20) observation were prepared by placing drops of the aqueous suspension onto carbon coated copper grids.

Atomic force microscopy (AFM) images were obtained with a Nanoscope Multimode and Explore atomic force microscope (Veeco Instruments, USA). All images were collected under ambient conditions at 50% relative humidity and 25 °C with a raster scanning rate of 1.8 Hz. Samples for the AFM images were prepared by depositing aqueous dispersions of GO or rGO onto a freshly cleaved mica surface using a drop-casting method. The samples were allowed to air dry under ambient conditions prior to being introduced into the TEM chamber for observation. The amount of In was obtained by inductively coupled plasma (ICP-9000(N + M), USA, Thermo Jarrell-Ash Corp).

2.6. Electrochemical measurement

The In_2O_3/rGO, carbon black, and PTFE with a mass ratio of 75:15:10 were mixed until homogeneous. Ethanol was then added to the mixture to form a paste. The paste was evenly coated on a piece of nickel foam (1 cm^2), and then dried and then pressed at a pressure of 6 MPa to give a tablet In_2O_3/rGO electrode pad. The mass loading of active materials for the electrode is about 8 mg.

The electrochemical activities of the In_2O_3/rGO hybrids were evaluated using CV and GV in 2 M KOH using a CHI660D electrochemical workstation (Shanghai Chen Hua). A three-electrode system was used with a large-area Ti plate as the auxiliary electrode, an Hg/HgO electrode as the reference electrode, and In_2O_3/rGO as the working electrode.

3. Results and discussion

3.1. Reduction of GO by In powder

GO was prepared from purified natural graphite by a modified Hummer's method. GO readily disperses in water with mild ultrasonic treatment to form a transparent brown suspension, which is stable for several months without precipitation occurring (Fig. 1a).

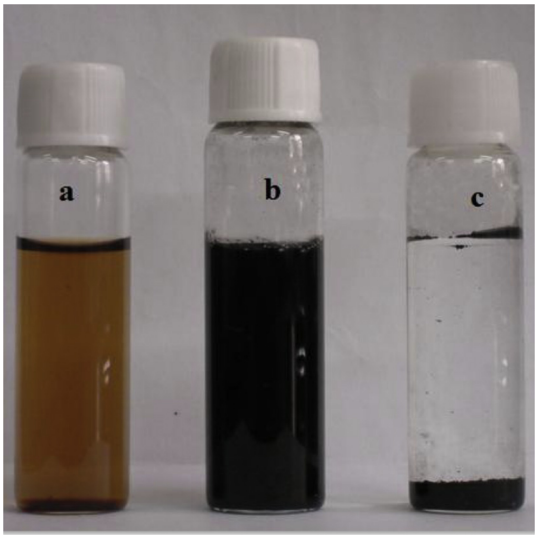

Fig. 1. Photographs of GO solution (a), rGO solution in the presence PVP (b) and rGO solution with no PVP (c).

GO can also be suspended in *N*,*N*-dimethyl formamide and dimethyl sulfoxide. The TEM and AFM images of GO shown in Figs. S1 and S2 respectively show that the GO nanosheets consist of one to several layers.

When In powder was added to the GO suspension in the presence of PVP and heated at 95 °C, the color of the GO solution gradually turned from brown to black (Fig. 1b), implying that GO was reduced by the In powder. However, when GO was reduced in the absent of PVP, the rGO precipitated from the solution (Fig. 1c). This is because GO becomes hydrophobic after the hydrophilic functional groups are removed [31].

The transition from GO to rGO can be monitored by UV–vis spectroscopy. The UV–vis absorption peak maximum of the GO dispersion is at 234 nm, which corresponds to the $\pi \rightarrow \pi^*$ transition [32]. This peak gradually red-shifted to 270 nm with a significant increase in intensity after the reaction, suggesting that GO was reduced and the electronic conjugation was restored. The position of the absorption peak maximum reflects the degree of the reduction in the rGO [31].

The effects of several factors such as pH, the mass ratio of In/GO and the reaction temperature on the reduction of GO by In powder were tested and the results are shown in Fig. 2. As shown in Fig. 2a, when the pH value was higher than 5, GO was only partially reduced since the absorption peak only shifted from 234.0 to around 260.0 nm. When the pH was 5.0, the absorption peak of the rGO suspension shifted to 270.0 nm. Further decreasing the pH value did not cause a further shift in the absorption peak, but required less reduction time. So GO can be efficiently reduced by In powder under acidic conditions. In order to facilitate operation, the pH was fixed at 1.

The reduction of GO at different In/GO ratios is shown in Fig. 2b. When the mass ratio of In/GO was 0.5:1, the absorption peak of the suspension was 260.0 nm, which indicates that GO was not completely reduced at this low In/GO ratio. When the mass ratio of In/GO was 1:1, the absorption peak of the rGO suspension was 270.0 nm, and a further increasing in the In/GO ratio did not result in a further peak shift. However, the reaction time was shortened with a higher ratio. For example, the reduction time is only 0.5 h at the In/GO ratio of 5:1. Therefore, 1:1 was chosen as the In/GO ratio for the reduction of GO.

Fig. 2c shows the influence of temperature on the GO reduction. When the reaction temperature was lower than 70 °C, the maximum absorption peak shifted from 234.0 to at most 265.0 nm, which is lower than that of rGO prepared at 80 °C (270.0 nm). When the reaction temperature was increased to 95 °C, the maximum absorption peak was still at 270 nm. Thus, 80 °C was the minimum reaction temperature for the reduction of GO by In powder. In order to prepare rGO in a short time, the selected conditions for GO reduction were: In/GO ratio = 1.0, pH = 1, 95 °C.

According to the above selected conditions, GO was reduced using In powder with no PVP. The reaction product was collected for analysis by centrifugation and repeatedly washed with distilled water to remove impurities. Finally, the black product was dried under vacuum at 50 °C for 12 h.

To characterize the structure of the GO reduced by In powder, XRD patterns of graphite, GO and rGO were measured and are shown in Fig. 3. Graphite has a narrow and strong diffraction peak at around $2\theta = 26.5°$ (002). However, in the GO spectrum, this peak disappears and a new broad peak at $2\theta = 11.34°$ (*d*-spacing is 0.78 nm) is present, which indicates that GO has an enlarged layered structure. The large interlayer distance is attributed to the formation of hydroxyl, epoxy and carboxyl groups which allows water molecules to intercalate between the layers and increases the distances between the layers [31]. The peak at 11.34° vanishes in the XRD of rGO which confirms the extensive reduction of GO by In powder.

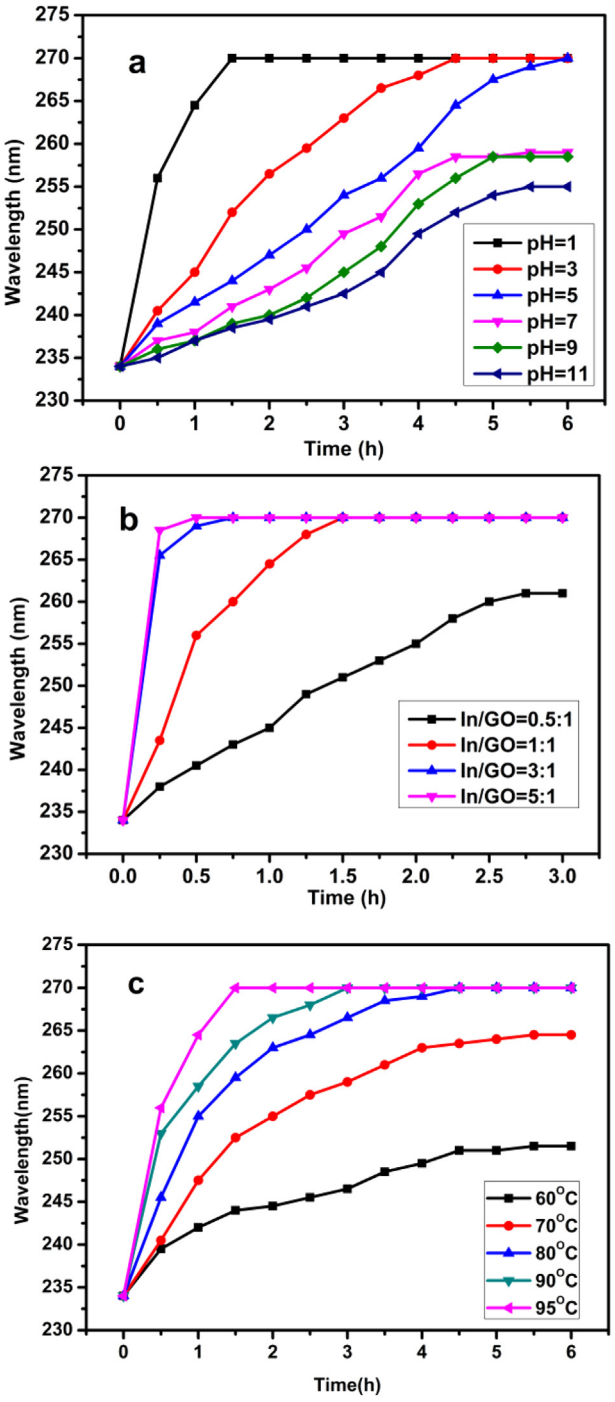

Fig. 2. Effect of GO suspension pH (a), the In/GO ratio (b), and the reaction temperature (c) on the reduction of GO by In powder. Unless otherwise stated In/GO = 1:1, temperature = 95 °C, pH = 1.

The thermal stabilities of graphite, GO and rGO were measured in a N_2 atmosphere and the results are shown in Fig. 4. Graphite does not show any mass loss from room temperature to 600 °C. GO has a 20% mass loss below 200 °C which is the result of the evaporation of absorbed water. It also has a rapid 20% mass loss from 200 to 250 °C where it gives off CO, CO_2 or steam when the oxygen-containing functional groups are removed [33]. The rGO only has a total mass loss of 10% and no mass loss below 250 °C is observed. This indicates that the thermal stability of rGO was dramatically improved which is due to a decrease in the amount of oxygen-

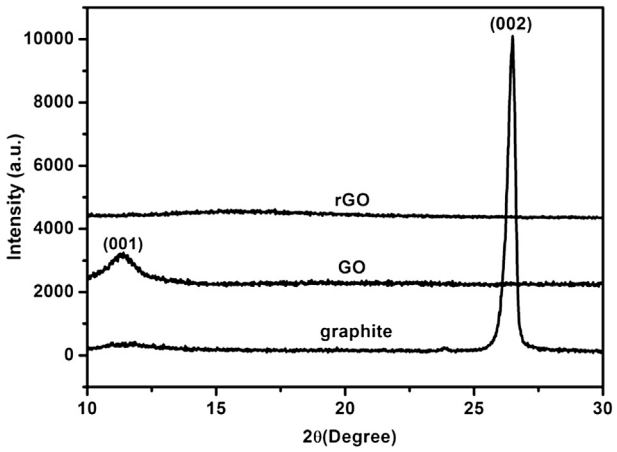

Fig. 3. XRD patterns of graphite, GO and rGO.

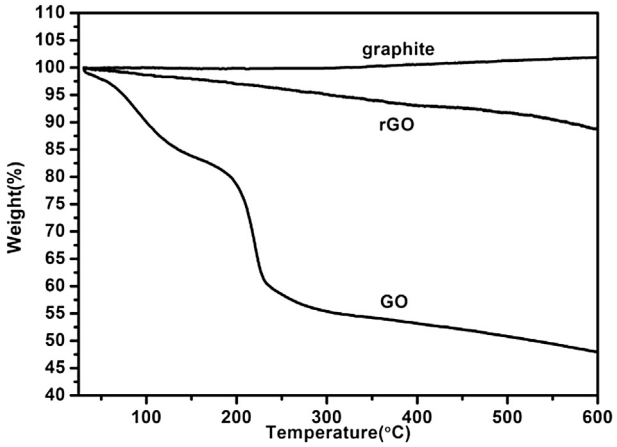

Fig. 4. TGA profiles of graphite, GO and rGO.

containing functional groups. So this data again indicates that the GO was effectively reduced by In powder.

Raman spectroscopy is a widely used and powerful tool to characterize the structural changes of graphene-based materials. The Raman spectrum of GO in Fig. 5 is characterized by two main features, a G band (the E2g mode of the sp^2 carbon atoms) at 1596 cm^{-1} and a D band (the symmetric A1g mode) at 1360 cm^{-1}. Changes in the relative intensities of the D and G bands (D/G) indicate changes in the electronic conjugation state of the GO during reduction [34,35]. As shown in Fig. 5, the D/G intensity ratio increased after reduction. Since the D/G intensity ratio is inversely proportional to the average size of the sp^2 domains, the higher ratio suggests that smaller in-plane sp^2 domains were formed during the reduction of GO [34,36]. This again demonstrates the reduction of GO by In powder.

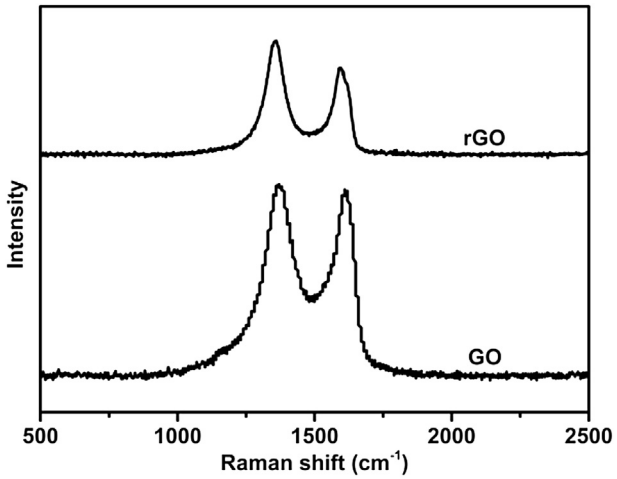

Fig. 5. Raman spectra of GO and rGO.

The reduction of GO was further quantitatively analyzed by XPS. The C1s spectra of rGO and GO are shown in Fig. 6 and Fig. S3, respectively. The C1s spectrum of GO can be deconvoluted into three peaks: C–C/C=C (284.4 eV), C–O (286.5 eV) and C=O (288.4 eV). As shown in Table 1, compared to GO, the rGO spectrum shows a large decrease in intensity at 286.2 eV and a simultaneous increase at 284.6 eV (C=C). These changes again indicate the removal of the oxygen-containing functional groups and the formation of a graphene backbone during the reduction. The atomic percentages of C and O in GO are about 74.1% and 25.9% respectively, whereas they are 90.9% and 9.1% respectively in rGO. The atomic ratio of carbon to oxygen (C/O) in GO is 2.9 whereas it is 10.0 in rGO. This significant increase also indicates the efficient removal of oxygen-containing functional groups [31].

The reduction of GO by several other metals has been reported and the C/O ratios for these rGO samples are shown in Table 2. The C/O ratio of 10.0 achieved with In is higher than all the other ratios listed in Table 2 except for that of the rGO reduced by Al. However, all these GO samples were reduced by the hydrogen spillover mechanism, in which the reducing agent was not the metal but rather hydrogen produced by the reaction of the metal and the acid. Therefore, these methods require large amounts of acid and metals to produce sufficient hydrogen. This produces problems in the post-treatment because the excess acid has to be removed, so from an environmental protection point of view, this is not a good method. However, the reduction in this work does not need additional acid because the pH of the GO solution in this work was about 3.0 and GO could be reduced using In powder at pH 3.0 (Fig. 2a). Even though the pH of the solution was fixed at 1.0 according to our selected conditions, a few additional acid is required compared with other metals. Therefore, the reduction of GO using In powder is environmentally friendly.

3.2. Fabrication of In_2O_3/rGO hybrids

The above studies confirm that In powder can be used to efficiently prepare rGO from GO. During the reduction of GO by the In powder, GO was reduced to rGO and the In powder may be oxidized to In^{3+} ions. In order to make use of the by-products In^{3+} ions, the ammonia water was introduced to transform In^{3+} ions to $In(OH)_3$, and then annealed at 300 °C to obtain In_2O_3/rGO hybrid. Some characterization methods were used to analyze the obtained In_2O_3/rGO hybrid.

Fig. 7 shows the XRD diagram of the In_2O_3/rGO hybrids. Obviously, the diffraction peak of GO at around $2\theta = 11.34°$ (Fig. 3) has disappeared, while a broad diffraction peak appears at 2θ of about 17.15° (d-spacing is 0.52 nm), revealing the reduction of GO [42]. The interlayer spacing changes from 0.78 nm for GO to 0.52 nm for rGO due to the disappearance of oxygen-containing functional groups. The diffraction peaks at $2\theta = 29.64°$, 34.68°, 44.6°, 50.48° and 60.16° are indexed with the In_2O_3 corresponding planes of (222), (400), (431), (440) and (622), respectively [43], indicating that the successful preparation of In_2O_3/rGO.

Fig. 8 shows the TEM images of the In_2O_3/rGO hybrids. As shown in Fig. 8a, many nanoparticles are on the surface of the graphene

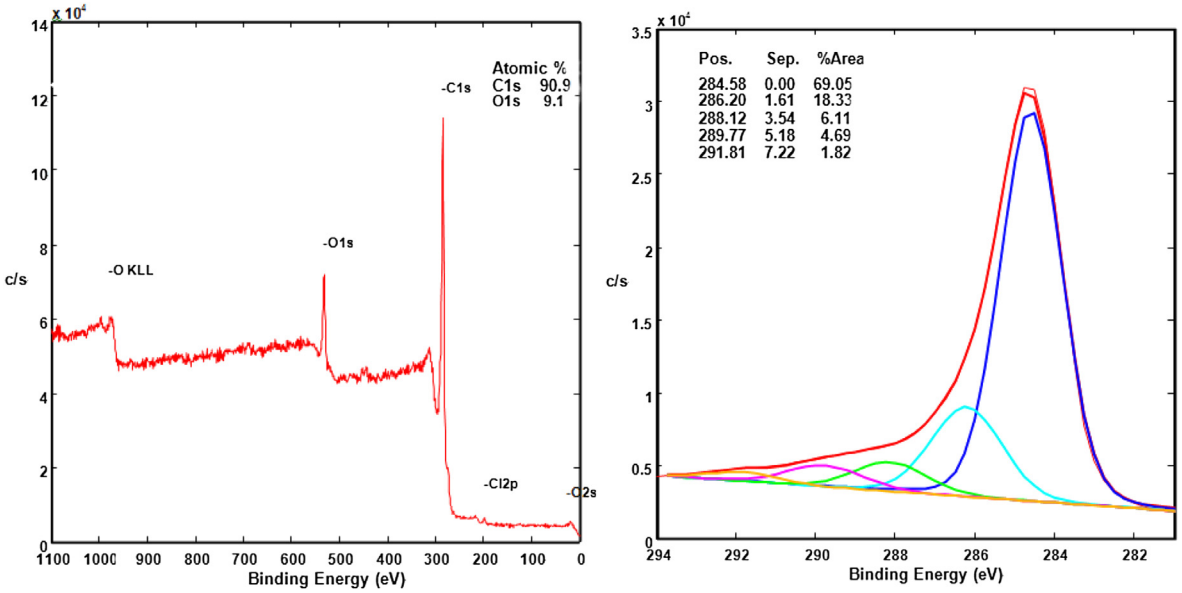

Fig. 6. The XPS and C1s spectra of rGO.

Table 1
Percentage of different bonds in GO and rGO.

Sample	Analysis			
GO	Carbon	Oxygen		C/O ratio
	74.1	25.9		2.9
	C=C	C–O	C=O	
	54.45	40.32	5.24	
rGO	Carbon	Oxygen		C/O ratio
	90.9	9.1		10.0
	C=C	C–O	C=O	
	69.05	18.33	6.11	

nanosheets. The high-resolution TEM image of the particles shows an obvious crystal lattice with an interplanar spacing of 0.27 nm (Fig. 8b), which is in good accordance with the reported literature value for that of In_2O_3 [43]. These results also confirm the formation of In_2O_3/rGO hybrids.

Fig. 9 shows the TGA curves of In_2O_3, rGO and the In_2O_3/rGO hybrid under flowing air. As shown in Fig. 9, there was no mass loss for the In_2O_3. The rGO was nearly completely combusted under air at about 550 °C, but owing to the presence of impurity, the rGO retained residual mass (6.6%). In the TGA curve of the In_2O_3/rGO hybrid, the residual mass of the In_2O_3/rGO hybrid was only 50.1% at 550 °C and it did not show any further decreasing from 550 to 700 °C. The amount of In_2O_3 in the In_2O_3/rGO hybrid can be calculated based on the TGA curve. So the mass percent (wt%) of In_2O_3 loading in the In_2O_3/rGO hybrid is about 43.5 wt%, which is similar with that obtained from ICP (45.2 wt%).

The above results have verified the formation of In_2O_3/rGO, which also proves the proposed mechanism for the reduction of GO and the formation of the hybrid (Fig. 10).

Table 2
C/O ratios of rGO prepared using different metals under acidic conditions.

Sample	Metal (M)	Amount of acid	M/GO (g g^{-1})	Acid/GO (g g^{-1})	C/O ratio	Ref.
rGO	Fe	20 mL of conc. HCl	2	14.6	7.9	[37]
rGO	Al	10 mL of conc. HCl	5	18.2	18.6	[38]
rGO	Zn	10 mL of conc. HCl	20	91.2	8.2	[39]
rGO	Ni	70 mL of conc. HCl	16.7	340.7	X	[40]
rGO	Mg	HCl	6.7	24.3	3.95	[41]

3.3. Electrochemical characterization

The electrochemical properties of In_2O_3/rGO were studied by CV and GV using a three-electrode system. Typical CV curves of the In_2O_3/rGO electrode with different scan rates in 2 M KOH aqueous solution are shown in Fig. 11a. The CV curves show an ideal rectangular shape, which indicates that there is good charge propagation within the electrode [44]. The shapes at high scan rates are similar to those at low scan rates with no obvious distortion, indicating a high-rate performance and excellent ionic and electronic transport within the electrode material [45].

The specific capacitances (SCs) based on the mass of the In_2O_3/rGO hybrid are shown in Fig. 11b. These values are 169, 149, 136.1 and 134.8 F g^{-1} for scan rates of 20, 50, 100 and 200 mV s^{-1}, respectively. The decrease in SC with scan rate is attributed to the fact that the electrolyte ions are unable to fully accessible the interior surfaces of the active materials because of the reduced diffusion time at higher scan rates [46].

The effect of the amount of In_2O_3 loading on the electrochemical performance at a scan rate of 20 mV s^{-1} was also studied and the CV

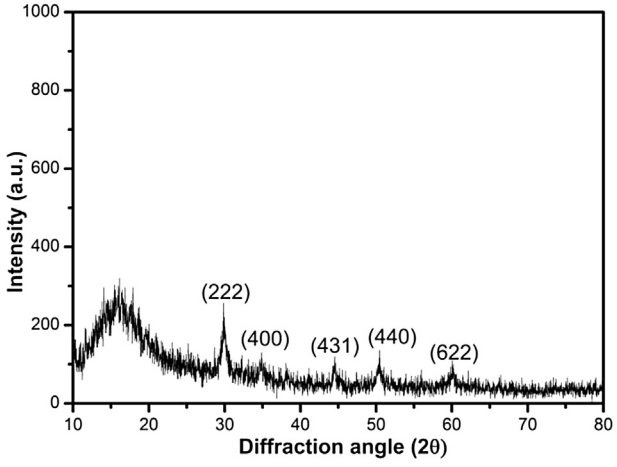

Fig. 7. XRD image of the In_2O_3/rGO hybrid.

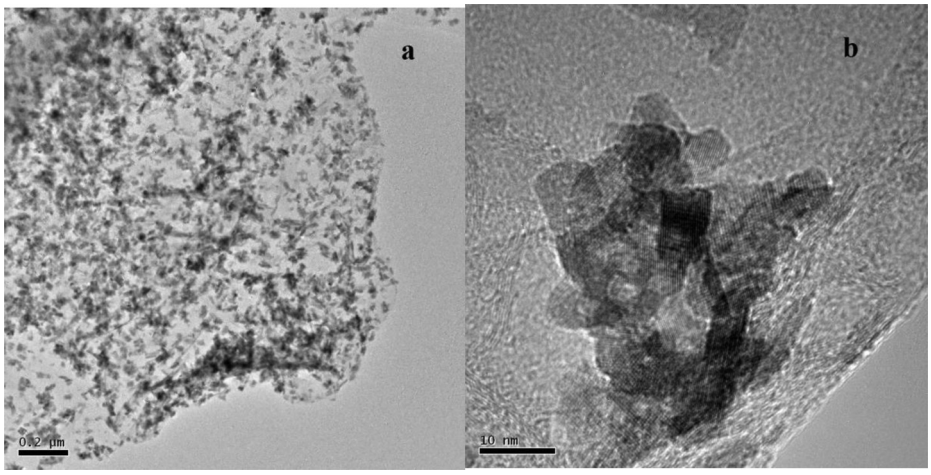

Fig. 8. TEM images of the In_2O_3/rGO hybrid.

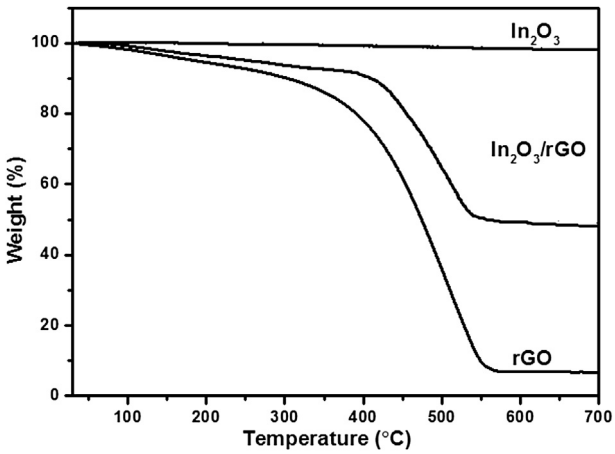

Fig. 9. TGA of the In_2O_3/rGO hybrid.

curves and SCs are shown in Fig. 11c and d. From 30.7% to 43.5% (In_2O_3 wt% in the In_2O_3/rGO hybrids), the SC increases, which is attributed to that the synergetic effect between rGO and In_2O_3 might improve the performance of supercapacitors. After that, the decrease of SC is observed for 56.5% and 64.6%, because some In_2O_3 nanoparticles anchored on the rGO are aggregated leading to decreased SC [47]. Meanwhile, the SCs of all the In_2O_3/rGO hybrids were higher than that of the pure rGO and pure In_2O_3, which is similar with that for Mn_3O_4/rGO [48] and CeO_2/carbon nanotube (CNT) [49] reported in the literature.

Moreover, the SC of In_2O_3/rGO is superior to that reported for other In_2O_3-based materials. For example, the SC of In_2O_3 nanoparticle/CNT was 64 F g^{-1} at a scan rate of 20 mV s^{-1} [50] and those of In_2O_3 nanospheres and nanorods were 7.6 and 105 F g^{-1} respectively at a scan rate of 50 mV s^{-1} [51]. The high SC may be attributed to the large specific surface area of the rGO which enlarges the interfacial area between the active materials and the electrolyte and to the high conductivity of rGO which facilitates the charge transfer of the poorly conductive In_2O_3 phase to enhance the electrode reactivity. Mentionable, the CV curves of sample In_2O_3/

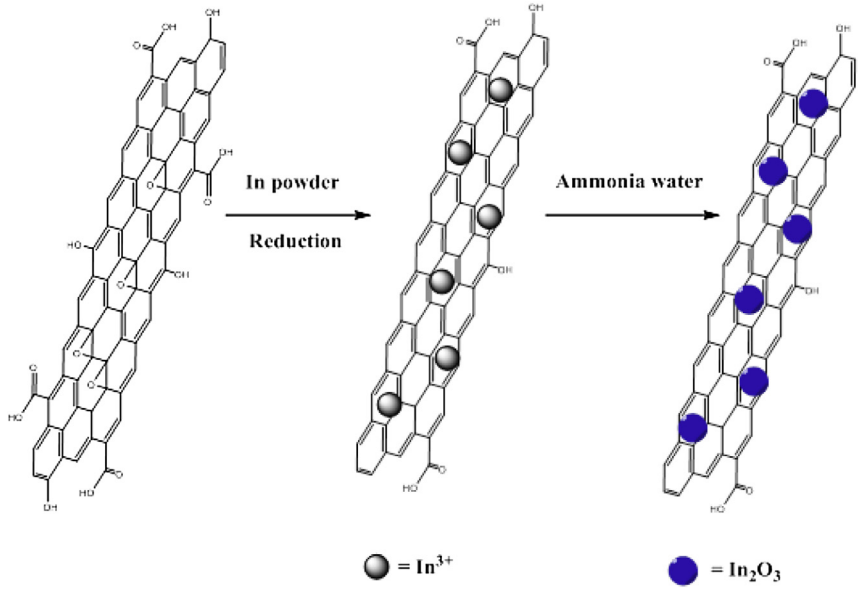

Fig. 10. Schematic representation of the In_2O_3/rGO hybrid formation.

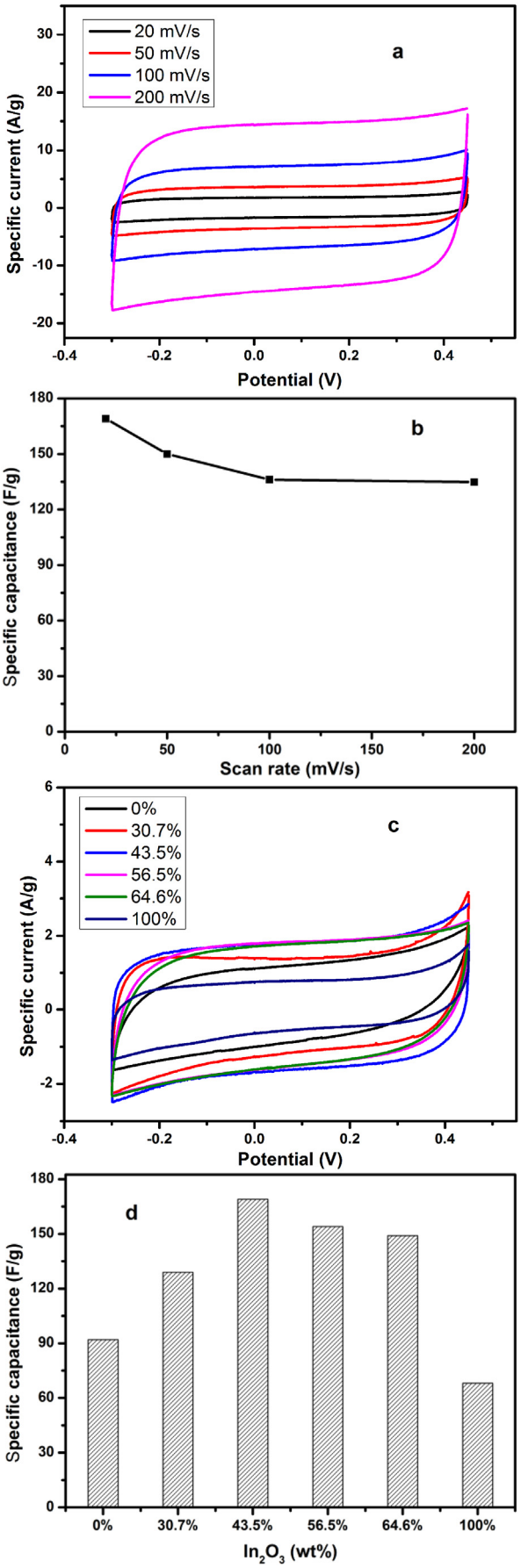

Fig. 11. CV curves (a) and SCs (b) of the In_2O_3/rGO hybrid with different scan rates; the CV curves (c) and SCs (d) of the In_2O_3/rGO (In_2O_3 wt% = 0%, 30.7%, 43.5%, 56.5%, 64.6% and 100%, respectively) hybrids at a scan rate of 20 mV s^{-1}.

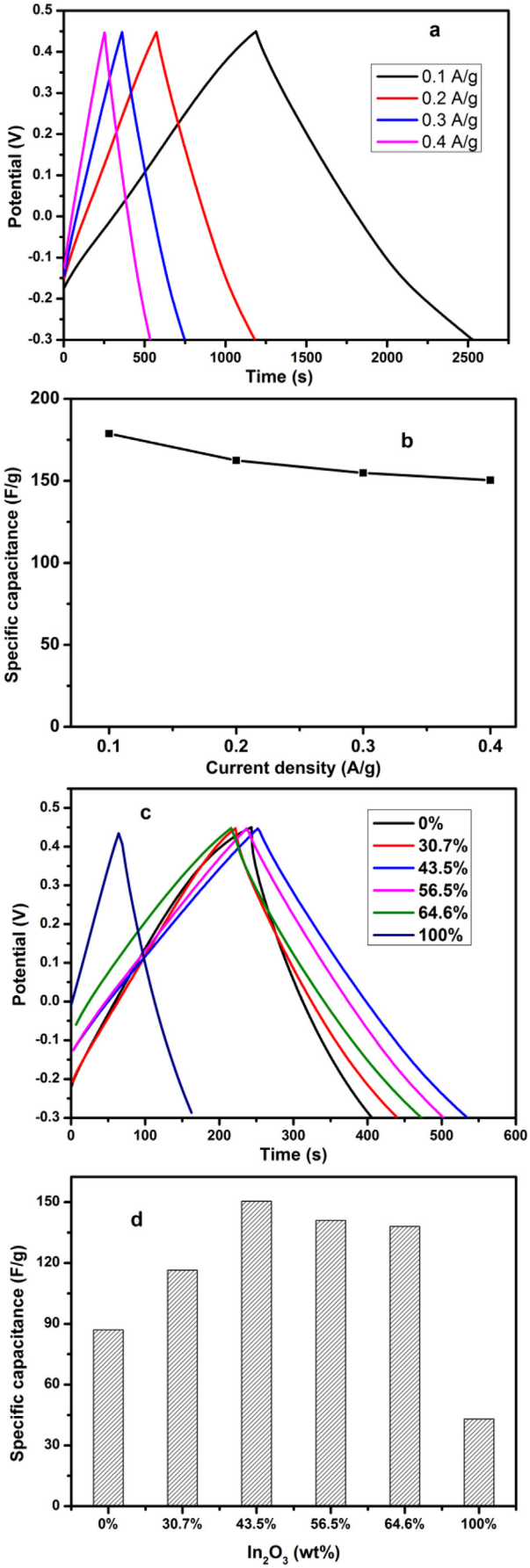

Fig. 12. GV curves (a) and SCs (b) of the In_2O_3/rGO hybrid at different current densities; GV curves (c) and SCs (d) of the In_2O_3/rGO (In_2O_3 wt% = 0%, 30.7%, 43.5%, 56.5%, 64.6% and 100%, respectively) hybrids at a current density of 0.4 A g^{-1}.

rGO and background Ni foam are shown in Fig. S4. They clearly demonstrate the capacitance contributed from Ni foam can be ignored. This was also confirmed by Wang et al. who reported that the capacitance contributed from Ni foam can be ignored when the used active material was more than 2 mg [47,52].

Fig. 12a shows the GV curves of the In_2O_3/rGO hybrid measured at different current densities. The GV curves of In_2O_3/rGO are linear and symmetric, which is a characteristic of an ideal capacitor that is capable of reversible charging and discharging [53]. The IR drops in all the curves are similar and small, indicating low resistance and good contact between the electrode material and the collectors [54]. The SCs of the In_2O_3/rGO hybrid were calculated from their GV curves and are shown in Fig. 12b. The SC of the In_2O_3/rGO hybrid was 178.8 F g^{-1} at a low current density of 0.1 A g^{-1}, and decreased to 150.4 F g^{-1} at a comparatively high current density of 0.4 A g^{-1}. This decrease with increasing current density can be explained by the slow diffusion and migration of the protons in the In_2O_3/rGO hybrid at high current density. At lower current densities, most of the active sites can be utilized for charge storage. However, at higher current densities, diffusion and migration hinder the transport of the protons due to time constraints and only the outer active surface can be utilized for charge storage [55]. Moreover, the SC of the In_2O_3/rGO is also higher than those of other In_2O_3-based materials reported in the literature. For example, the SC of the In_2O_3 nanoparticle/CNT was about 64 F g^{-1} at a current density of 0.5 A g^{-1} [50].

The GV curves and SCs of the In_2O_3/rGO hybrids (different amount of In_2O_3) at a current density of 0.4 A g^{-1} are shown in Fig. 12c and d. As shown in Fig. 12d, the SC of the In_2O_3/rGO hybrids depends on the mass percent of In_2O_3 and the In_2O_3/rGO (In_2O_3 wt % = 43.5%) hybrid shows the highest among these In_2O_3/rGO hybrids, which is in good accordance with the results obtained from CV. Therefore, the GV further proves that the rGO can be served as a good support for In_2O_3.

To exploit the application of the In_2O_3/rGO hybrid as supercapacitor electrode materials, the capacitance retention was measured for 5000 charge/discharge cycles at a current density of 4 A g^{-1} and the results are shown in Fig. 13. After 5000 charge/discharge cycles, the In_2O_3/rGO electrode retained about 93.7% of its initial capacitance, indicating good cycle-life stability. Capacity loss with extended cycling is a common phenomenon in supercapacitors. For instance, the In_2O_3 nanoparticle/CNT reported by Chen et al. retained about 88% of its initial capacitance after a 500-cycle charge/discharge [50]. The decay of the SC with extended cycling may be attributed to damage in the structure of the electrode [56]. For the In_2O_3/rGO hybrid, the slight decay in the SC could be ascribed to the fact that the rGO could inhibit aggregation of the In_2O_3 nanoparticles. This high capacitance retention indicates that the In_2O_3/rGO hybrid should be highly durable for electrochemical capacitor applications in mild aqueous electrolytes [57].

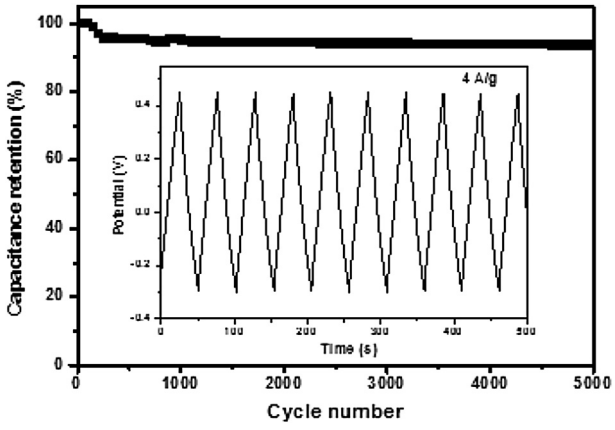

Fig. 13. Capacitance retention of the In_2O_3/rGO hybrid at a constant current density of 4 A g^{-1}. The inset shows the charge–discharge curves of the In_2O_3/rGO hybrid.

4. Conclusions

A simple and rapid route for the chemical reduction of GO using In powder as a reductant has been developed. The reduction conditions for the reduction of GO in terms of pH, temperature and In/GO ratio were determined. The reduction was complete in about 30 min. The In^{3+} ions, the by-products during the reaction between GO and In powder, were easily transformed to In_2O_3 nanoparticles on the rGO nanosheets. The prepared In_2O_3/rGO hybrids were used as electrode materials in supercapacitors and showed excellent electrochemical performance with a high SC and good stability.

Acknowledgments

This work was supported by the National Natural Science Foundation of China (21074089, 21276181).

Appendix A. Supplementary data

Supplementary data related to this article can be found at http://dx.doi.org/10.1016/j.jpowsour.2014.05.051.

References

[1] A.K. Geim, K.S. Novoselov, Nat. Mater. 6 (2007) 183.
[2] K.S. Novoselov, A.K. Geim, S.V. Morozov, D. Jiang, M.I. Katsnelson, I.V. Grigorieva, S.V. Dubonos, A.A. Firsov, Nature 438 (2005) 197.
[3] A.A. Balandin, S. Ghosh, W. Bao, I. Calizo, D. Teweldebrhan, F. Miao, C.N. Lau, Nano Lett. 8 (2008) 902.
[4] S. Stankovich, D.A. Dikin, G.H.B. Dommett, K.M. Kohlhaas, E.J. Zimney, E.A. Stach, R.D. Piner, S.T. Nguyen, R.S. Ruoff, Nature 442 (2006) 282.
[5] D.A. Dikin, S. Stankovich, E.J. Zimney, R.D. Piner, G.H.B. Dommett, G. Evmenenko, S.T. Nguyen, R.S. Ruoff, Nature 448 (2007) 457.
[6] D. Li, R.B. Kaner, Science 320 (2008) 1170.
[7] C. Lee, X. Wei, J.W. Kysar, J. Hone, Science 321 (2008) 385.
[8] K.S. Novoselov, A.K. Geim, S.V. Morozov, D. Jiang, Y. Zhang, S.V. Dubonos, I.V. Grigorieva, A.A. Firsov, Science 306 (2004) 666.
[9] P.K. Ang, W. Chen, A.T.S. Wee, K.P. Loh, J. Am. Chem. Soc. 130 (2008) 14392.
[10] T. Kudo, Y. Ikeda, T. Watanabe, M. Hibino, M. Miyayama, H. Abe, K. Kajita, Solid State Ionics 152–153 (2002) 833.
[11] X. Wang, L.J. Zhi, K. Müllen, Nano Lett. 8 (2008) 323.
[12] C. Berger, Z.M. Song, T.B. Li, X.B. Li, A.Y. Ogbazghi, R. Feng, Z.T. Dai, A.N. Marchenkov, E.H. Conrad, P.N. First, W.A. Heer, J. Phys. Chem. B 108 (2004) 19912.
[13] T. Aizawa, R. Souda, S. Otani, Y. Ishizawa, C. Oshima, Phys. Rev. Lett. 64 (1990) 768.
[14] K.S. Kim, Y. Zhao, H. Jang, S.Y. Lee, J.M. Kim, K.S. Kim, J.H. Ahn, P. Kim, J.Y. Choi, B.H. Honget, Nature 457 (2009) 706.
[15] H.C. Schniepp, J.L. Li, M.J. McAllister, M. Sai, M. Herrera-Alonso, D.H. Adamson, R.K. Prud'homme, R. Car, D.A. Saville, I.A. Aksay, J. Phys. Chem. B 110 (2006) 8535.
[16] M. Lotya, Y. Hernandez, P.K. King, R.J. Smith, V. Nicolosi, L.S. Karlsson, F.M. Blighe, S. De, Z.M. Wang, I.T. McGovern, G.S. Duesberg, J.N. Coleman, J. Am. Chem. Soc. 131 (2009) 3611.
[17] Y. Hernandez, V. Nicolosi, M. Lotya, F.M. Blighe, Z.Y. Sun, S. De, I.T. McGovern, B. Holland, M. Byrne, Y.K. Gun'Ko, J.J. Boland, P. Niraj, G. Duesberg, S. Krishnamurthy, R. Goodhue, J. Hutchison, V. Scardaci, A.C. Ferrari, J.N. Coleman, Nat. Nanotechnol. 3 (2008) 563.
[18] H.L. Wang, J.T. Robinson, X.L. Li, H.J. Dai, J. Am. Chem. Soc. 131 (2009) 9910.
[19] V.H. Pham, T.V. Cuong, T.D. Nguyen-Plan, H.D. Pham, E.J. Kim, S.H. Hur, E.W. Shin, S. Kim, J.S. Chung, Chem. Commun. 46 (2010) 4375.
[20] X.F. Gao, J. Jang, S. Nagase, J. Phys. Chem. C 114 (2010) 832.
[21] Y.Y. Zhao, Y.K. Zhou, R. O'Hayre, Z.P. Sha, J. Phys. Chem. Solids 7 (2013) 1608.
[22] G.X. Wang, X.P. Shen, B. Wang, J. Yao, J. Park, Carbon 47 (2009) 1359.
[23] H.J. Shin, K.K. Kim, A. Benayad, S.M. Yoon, H.K. Park, I.S. Jung, M.H. Jin, H.K. Jeong, J.M. Kim, J.Y. Choi, Y.H. Lee, Adv. Funct. Mater. 19 (2009) 1987.
[24] Y.Q. Guo, X.Y. Sun, Y. Liu, W. Wang, H.X. Qiu, J.P. Gao, Carbon 50 (2012) 2513.

[25] M.J. Fernández-Merino, L. Guardia, J.I. Paredes, S. Villar-Rodil, P. Solís-Fernández, A. Martínez-Alonso, J.M.D. Tascón, J. Phys. Chem. C 114 (2010) 6426.
[26] C.Z. Zhu, S.J. Guo, Y.X. Fang, S.J. Dong, ACS Nano 4 (2010) 2429.
[27] Y. Wang, Z.X. Shi, J. Yin, ACS Appl. Mater. Interfaces 3 (2011) 1127.
[28] P.G. Ren, D.X. Yan, X. Ji, T. Chen, Z.M. Li, Nanotechnology 22 (2011) 055705.
[29] W. Hummer, R. Offeman, J. Am. Chem. Soc. 80 (1958) 1339.
[30] N.N. Zhang, H.X. Qiu, Y. Liu, W. Wang, Y. Li, X.D. Wang, J.P. Gao, J. Mater. Chem. 21 (2011) 11080.
[31] T. Wu, J.P. Gao, X.Y. Xu, W. Wang, C.J. Gao, H.X. Qiu, Nanotechnology 24 (2013) 215604.
[32] T. Wu, X.R. Wang, H.X. Qiu, J.P. Gao, W. Wang, Y. Liu, J. Mater. Chem. 22 (2012) 4772.
[33] G.X. Wang, J. Yang, J. Park, X.L. Gou, B. Wang, H. Liu, J.N. Yao, J. Phys. Chem. C 112 (2008) 8192.
[34] S. Stankovich, D.A. Dikin, R.D. Piner, K.A. Kohlhaas, A. Kleinhammes, Y. Jia, Y. Wu, S.T. Nguye, R.S. Ruoff, Carbon 45 (2007) 1558.
[35] F. Tuinstra, J.L. Koenig, J. Chem. Phys. 53 (1970) 1126.
[36] A. Ferrari, Solid State Commun. 143 (2007) 47.
[37] Z.J. Fan, W. Kai, J. Yan, T. Wei, L.J. Zhi, J. Feng, Y.M. Ren, L.P. Song, F. Wei, ACS Nano 5 (2011) 191.
[38] Z. Fan, K. Wang, T. Wei, J. Yan, L. Song, B. Shao, Carbon 48 (2010) 1670.
[39] P.B. Liu, Y. Huang, L. Wang, Mater. Lett. 91 (2013) 125.
[40] V.H. Pham, H.D. Pham, T.T. Dang, S.H. Hur, E.J. Kim, B.S. Kong, S. Kim, J.S. Chung, J. Mater. Chem. 22 (2012) 10530.
[41] Y.Z. Liu, Y.F. Li, M. Zhong, Y.G. Yang, W.Y.F. en, M.Z. Wang, J. Mater. Chem. 21 (2011) 15449.
[42] H.M.A. Hassan, V. Abdelsayed, A.E.R.S. Khder, K.M. AbouZeid, J. Terner, M.S. El-Shall, S.I. Al-Resayes, A.A. El-Azhary, J. Mater. Chem. 19 (2009) 3832.
[43] X.H. Liu, L.B. Zhou, R. Yi, N. Zhang, R.R. Shi, G.H. Gao, G.Z. Qiu, J. Phys. Chem. C 112 (2008) 18426.
[44] K. Zhang, L.L. Zhang, X.S. Zhao, J.S. Wu, Chem. Mater. 22 (2010) 1392.
[45] S. Biswas, L.T. Drzal, Chem. Mater. 22 (2010) 5667.
[46] J.G. Wang, Y. Yang, Z.H. Huang, F.Y. Kang, J. Mater. Chem. 22 (2012) 16943.
[47] L. Wang, X.H. Wang, X.P. Xiao, F.G. Xu, Y.J. Sun, Z. Li, Electrochim. Acta 111 (2013) 937–945.
[48] L. Li, Z.A. Hu, Y.Y. Yang, P.J. Liang, A.L. Lu, H. Xu, Y.Y. Hu, H.Y. Wu, Chin. J. Chem. 31 (2013) 1290–1298.
[49] R.S. Kalubarme, Y.H. Kim, C.J. Park, Nanotechnology 24 (2013) 365401.
[50] P.C. Chen, G.Z. Shen, S. Sukcharoenchoke, C.W. Zhou, Appl. Phys. Lett. 94 (2009) 043113.
[51] J.H. Chang, W. Lee, R.S. Mane, B.W. Cho, S.H. Han, Electrochem. Solid-State Lett. 11 (2008) A9–A11.
[52] W. Xing, S.Z. Qiao, X.Z. Wu, X.L. Gao, J. Zhou, S.P. Zhou, S.B. Hartono, D. Hulicova-Jurcakova, J. Power Sources 196 (2011) 4123–4127.
[53] G.X. Wang, Q.Q. Tang, H. Bao, X.W. Li, G.C. Wang, J. Power Sources 241 (2013) 231.
[54] X. Feng, Z.Z. Yan, N.N. Chen, Y. Zhang, Y.W. Ma, X.F. Liu, Q.L. Fan, L.H. Wang, W. Huang, J. Mater. Chem. A, http://dx.doi.org/10.1039/C3TA12780J.
[55] Y.G. Wang, L. Yu, Y.Y. Xia, J. Electrochem. Soc. 153 (2006) A743.
[56] Y. Wang, S.L. Gai, N. Niu, F. He, P.P. Yang, J. Mater. Chem. A 1 (2013) 9083.
[57] C. Portet, P.L. Taberna, P. Simon, Electrochim. Acta 49 (2004) 905.